Inorganic Chemistry
Article
Cite This: Inorg. Chem. 2019, 58, 10417−10423
pubs.acs.org/IC

Synthesis and Magneto-Structural Characterization of $Yb_3(OH)_7SO_4·H_2O$: a Frustrated Quantum Magnet with Tunable Stacking Disorder

Ningxin Jiang,[†] Xiaojian Bai,[‡] John Bacsa,[†] Martin Mourigal,[‡] and Henry S. La Pierre*[,†,§]

[†]School of Chemistry and Biochemistry, [‡]School of Physics, and [§]Nuclear and Radiological Engineering Program, Georgia Institute of Technology, Atlanta, Georgia 30332-0400, United States

Supporting Information

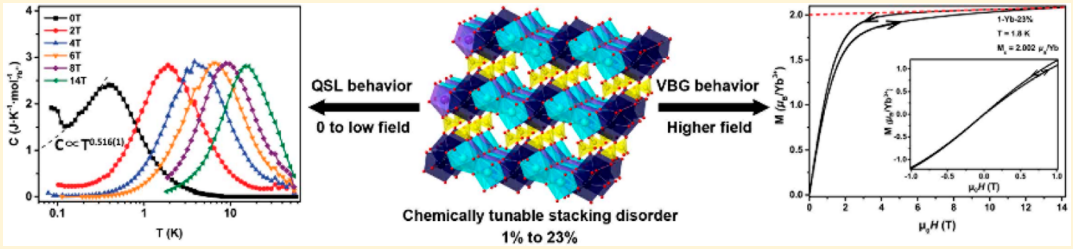

ABSTRACT: The quenched structural disorder in frustrated magnets can lead to apparent quantum spin liquid (QSL) behavior or to a valence bond glass state: the transition between these thermodynamic states has not been demonstrated experimentally. Herein, we report the synthesis of a novel layered rare earth hydroxide $Yb_3(OH)_7SO_4·H_2O$ as single crystals. The interplay between the strong distortion of the triangular lattice and low point group symmetry of the three distinct Yb^{3+} sites leads to quenched disorder. The variable stacking disorder in $Yb_3(OH)_7SO_4·H_2O$ is elucidated by comparison to the lutetium analogue, $Lu_3(OH)_7SO_4·H_2O$. The degree of disorder in $Yb_3(OH)_7SO_4·H_2O$ is controlled by the chemical form of the starting material and solution pH. In a low magnetic field, $Yb_3(OH)_7SO_4·H_2O$ displays QSL behavior, while, under a high field, a valence bond glass state is observed. The degree of stacking fault disorder in $Yb_3(OH)_7SO_4·H_2O$ modulates the observed magnetic properties and the transition between QSL and valence bond glass states.

INTRODUCTION

A quantum spin-liquid (QSL) is an exotic form of magnetism popularized by Anderson's conjecture that a resonating valence-bond (RVB) liquid[1] may be at the origin of unconventional superconductivity in copper oxides.[2] The elucidation of QSLs in real materials has since evolved into an independent quest.[3] It is noteworthy that highly entangled spins in the absence of magnetic order were first proposed for a two-dimensional (2D) Heisenberg model of frustrated nearest-neighbor (NN) exchange on the triangular lattice.[1] Several quasi-2D compounds such as $ZnCu_3(OH)_6Cl_2$, $EtMe_3Sb[Pd(dmit)_2]_2$, and α-$RuCl_3$ have emerged as promising QSL candidates.[4−8]

Recently, a 2D QSL candidate comprising *f*-element spin carriers, $YbMgGaO_4$ (YMGO), has been synthesized.[9] Several promising QSL-like phenomena are observed in the specific heat, neutron scattering, and muon spin rotation studies for YMGO.[10,11] However, Yb^{3+} ions are displaced away from the triangular plane due to the intrinsic site mixing between Mg^{2+} and Ga^{3+}. This structural feature can be regarded to introduce quenched disorder and was proposed to be the origin of the QSL phenomenology in YMGO.[12,13] However, a recent theoretical work suggests that the quenched disorder in YMGO may induce the formation of a valence bond glass (VBG) state, a glassy phase which is characterized by long-range valence bond correlation and not related to magnetic ordering.[14,15] The possibility of a VBG state in YMGO is reinforced by the observation of the spin freezing signatures in the ac susceptibility measurement.[16] The quenched disorder and the bond randomness are not uncommon in the frustrated magnets and are proposed to be important for the emergence of spin glass or VBG state.[15,17] Therefore, the synthesis of an analogous model compound with a similar triangular lattice but a stronger quenched disorder is ideal for understanding the role that quenched disorder plays in engendering a VBG state and the correlated thermodynamic signatures of a QSL.

Varying types and degrees of structural disorder are also found in other frustrated magnets.[18] For example, in $ZnCu_3(OH)_6Cl_2$, substitutional disorder results from some of the Zn^{2+} sites between layers occupied by Cu^{2+}.[19] These different types of disorder have a strong impact on the physical properties in these systems including the observed QSL phenomenology.[18,20,21] Recently, an iridate with significant stacking fault disorder, $H_3LiIr_2O_6$, was proposed as a QSL, but the relationship between the stacking disorder and the QSL behaviors is still unclear experimentally.[22−24] Therefore,

Received: June 5, 2019
Published: July 15, 2019

DOI: 10.1021/acs.inorgchem.9b01674
Inorg. Chem. 2019, 58, 10417−10423

synthesis of a frustrated magnet with a tunable degree of stacking disorder is necessary.

The triangular lattice is the paradigm of a geometric frustrated lattice. Layered rare-earth hydroxides (LRHs), as a group of 2D materials with a strongly distorted triangular lattice and low point group symmetry for lanthanide sites, enable the existence of complex magnetic exchange pathways which can structurally enforce quenched disorder. Therefore, the LRHs are an ideal platform to search for lanthanide-based frustrated magnets and study the relationship between the quenched disorder, QSL behavior, and VBG state.[25] The LRHs have the general formula $(Ln^{3+})_2(OH^-)_{6-m}(A^{n-})_{m/n}\cdot xH_2O$, where Ln is a trivalent lanthanide metal cation, A is an anion such as NO_3^- or SO_4^{2-}, and m is generally 1 or 2.[26,27] However, LRHs are typically prepared in powder form, which hinders the precise determination of crystal structure and, in the context of this study, the structural correlation to QSL behaviors.

Herein, a novel LRH, $Yb_3(OH)_7SO_4\cdot H_2O$, **1-Yb**, has been synthesized as phase-pure single crystals by hydrothermal methods. The stacking disorder in this material is elucidated by comparison to its lutetium analog, $Lu_3(OH)_7SO_4\cdot H_2O$, **1-Lu**. The degree of stacking disorder in **1-Yb** can be tuned by changing the starting materials, the associated rate of dissolution, and olation under reaction conditions. Magnetic susceptibility and specific heat measurements show that no spin ordering occurs down to 0.08 K and that the magnetic ground state of Yb^{3+} ions is an effective spin-1/2 Kramer's doublet. These observations suggest, in conjunction with heat capacity studies, that **1-Yb** displays QSL behaviors at lower field. Evidence for the existence of VBG state is also observed under a high magnetic field. Glassy behavior is magnified in the samples with a higher degree of stacking disorder, which suggests that the observed VBG state is correlated both with the distortion of the triangular lattice and stacking fault disorder.

MATERIALS AND METHODS

General Methods. All reagents were obtained from commercial suppliers without further purification. Deionized water with a resistivity of 18.2 MΩ·cm was used for all syntheses. Hydrothermal reactions were carried out in 23 and 10 mL Teflon-lined pressure vessels (Parr 4749) purchased from Parr Instruments.

Synthesis of $Yb_3(OH)_7SO_4\cdot H_2O$ (1-Yb). Single crystals of $Yb_3(OH)_7SO_4\cdot H_2O$ were synthesized by a conventional hydrothermal method. A mixture of 394.1 mg of Yb_2O_3 (1.0 mmol), 697.0 mg of K_2SO_4 (4.0 mmol), 53.4 μL of 98% H_2SO_4, and 8.95 mL deionized water was sealed in a stainless-steel Parr vessel equipped with a 23 mL Teflon liner. The Parr vessel was put in a preheated gravity convection lab oven at 210 °C for 2 days under autogenous pressure and then cooled to room temperature at a rate of 5 °C/h. Colorless prismatic crystals were isolated from the liner by filtration, washed with deionized water and ethanol sequentially, and dried in the air for 1 day to afford 338 mg of the title compound (yield 67% based on Yb^{3+}). The water content in $Yb_3(OH)_7SO_4\cdot H_2O$ was determined by crystallography and isothermal TGA. Bulk purity was determined by PXRD (Figure S5).

Synthesis of $Lu_3(OH)_7SO_4\cdot H_2O$ (1-Lu). Single crystals of $Lu_3(OH)_7SO_4\cdot H_2O$ were synthesized using a conventional hydrothermal method. A mixture of 199.0 mg of Lu_2O_3 (0.5 mmol), 348.5 mg of K_2SO_4 (2.0 mmol), 32.0 μL of 98% H_2SO_4, and 4.00 mL deionized water were sealed in a stainless-steel Parr vessel equipped with a 10 mL Teflon liner. The Parr vessel was put in a preheated gravity convection lab oven at 210 °C for 2 days under autogenous pressure and then cooled to room temperature at a rate of 5 °C/h. Colorless prismatic crystals were isolated from the liner by filtration, washed with deionized water and ethanol sequentially, and dried in air for 1 day to afford 173 mg of $Lu_3(OH)_7SO_4\cdot H_2O$ (yield 68% based on Lu^{3+}). The water content in the $Lu_3(OH)_7SO_4\cdot H_2O$ was determined by crystallography. Bulk purity was determined by PXRD (Figure S6).

Synthesis of $Yb_2(SO_4)_3\cdot 8H_2O$. A mixture of 1.576 g of Yb_2O_3 (4.0 mmol), 1.28 mL of 98% H_2SO_4 (24.0 mmol), and 3.2 mL deionized water was sealed in a stainless-steel Parr vessel equipped with a 23 mL Teflon liner. The Parr vessel was put in a preheated gravity convection lab oven at 210 °C for 12 h under autogenous pressure and then cooled to room temperature slowly in the oven. The crystals were isolated from the liner by filtration, washed with deionized water and ethanol sequentially, and dried in the air for 2 h to afford 3.57 g of the title compound (yield 57% based on Yb^{3+}). Bulk purity was determined by PXRD (Figure S7)

Synthesis of $Yb_3(OH)_7SO_4\cdot H_2O$ with 23% Stacking Disorder (1-Yb-23%). Single crystals of $Yb_3(OH)_7SO_4\cdot H_2O$ with 23% stacking disorder (**1-Yb-23%**) were synthesized by a hydrothermal method. A mixture of 778.4 mg of $Yb_2(SO_4)_3\cdot 8H_2O$ (1.0 mmol), 348.5 mg of K_2SO_4 (2.0 mmol), 1.1 mL of 5.0 M KOH aqueous solution, and 8.8 mL of deionized water was added to a 23 mL Teflon liner. The reaction mixture was stirred with a Teflon stir bar in the air for 15 min. The stir bar was removed from the solution, and the Teflon liner was placed in a stainless-steel Parr vessel. The sealed Parr vessel was put in a preheated gravity convection lab oven at 210 °C for 18 h under autogenous pressure and then cooled to room temperature at a rate of 10 °C/h in the oven. The colorless crystals were isolated from the liner by filtration, washed with deionized water and ethanol sequentially, and dried in the air for 1 day to afford 156 mg of product (yield 62% based on Yb^{3+}). The water content in the $Yb_3(OH)_7SO_4\cdot H_2O$ was determined by crystallography. Bulk purity was determined by PXRD (Figure S8).

Single Crystal X-ray Diffraction. Single crystals of all compounds were adhered to Mitogen loops with Paratone oil and then mounted on a goniometer under a cold stream at 100 K (for **1-Yb-252 K**, the temperature was 252 K). The crystals were then optically aligned on a Bruker D8 Quest X-ray diffractometer using a digital camera. Diffraction data were obtained by with an X-ray source (Mo Kα, λ = 0.71073 Å) with high brilliance and high-performance focusing multilayered optics. APEX 3 was used for determination of the unit cells, data collection, and integration of the data. Numerical absorption corrections were also applied with SADABS.[28] A hemisphere of data was collected for all crystals. The structure was solved using the ShelXT structure solution program using the Intrinsic Phasing solution method and by using Olex2 as the graphical interface.[29] The model was refined with version 2014/7 of ShelXL2014 using Least Squares minimization.[30]

Powder X-ray Diffraction (PXRD). Powder X-ray diffraction (PXRD) patterns were obtained with a PANalytical X'Pert PRO Alpha-1 diffractometer using a 1.8 kW ceramic copper tube source. The simulations of PXRD patterns from SCXRD results are performed using software CrystalDiffract 6.

Fourier-Transformation Infrared Spectroscopy (FT-IR). Infrared (IR) samples were acquired as powders on a Bruker ALPHA FTIR spectrometer from 400 to 4000 cm^{-1} in an inert atmosphere box (Vigor) under a dinitrogen (<0.1 ppm of O_2/H_2O) atmosphere. The sample was dried under a vacuum using Schlenk techniques for 2 h prior to the FT-IR measurement.

Physical Property Measurements and Data Processing. DC magnetic susceptibility measurements and isothermal magnetization measurements M(H) were performed on **1-Yb** and **1-Yb-23%** using a PPMS vibrating sample magnetometer in a range of magnetic fields $0 \le \mu_0 H \le 14$ T and temperatures $1.8 \le T \le 300$ K. AC magnetic susceptibility measurements were performed on **1-Yb** and **1-Yb-23%** using a PPMS AC measurement system in magnetic fields of 0 T in the temperature range of $1.8 \le T \le 10$ K varying AC frequency from 10 Hz to 9984 Hz. The Curie–Weiss temperature θ_{cw} was derived from the linear fit of data within a range with the Curie–Weiss law.

DOI: 10.1021/acs.inorgchem.9b01674
Inorg. Chem. 2019, 58, 10417–10423

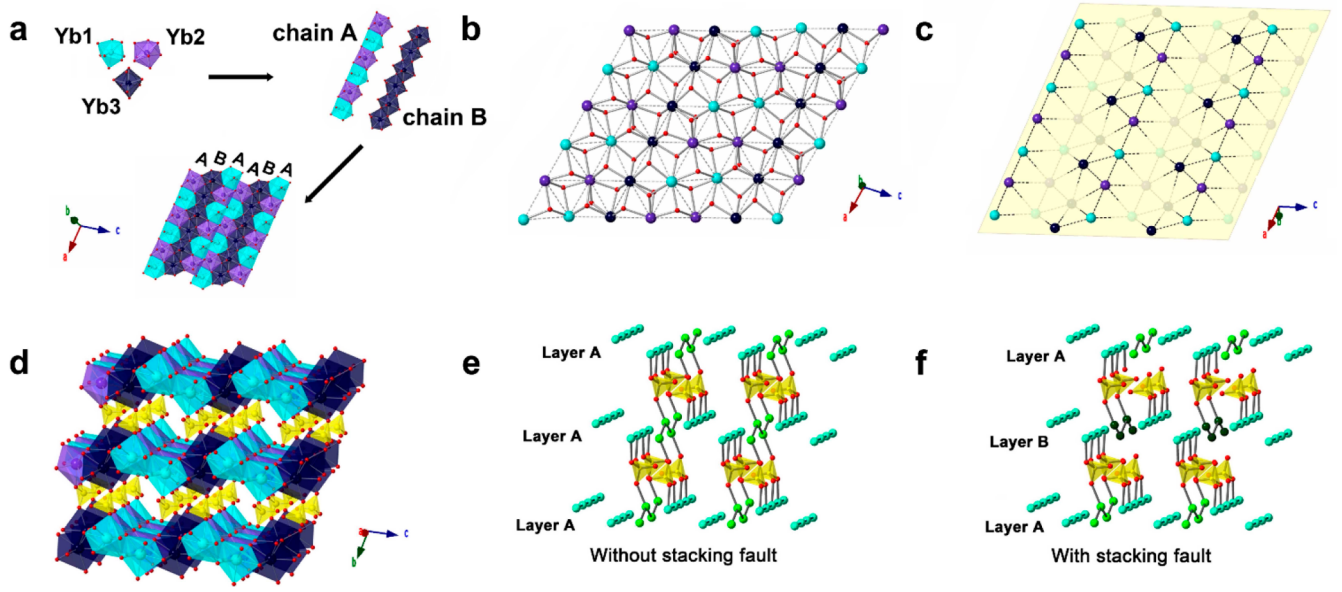

Figure 1. (a) Three types of YbO_8 polyhedra, chain A, chain B, and 2D-layer in **1-Yb**. (b) Top view of the layer with a triangular lattice. (c) The wave-like feature of the layer with (010) lattice plane (marked in beige) as a reference. (d) Layered structure of **1-Yb** along the *a* axis. Demonstration of stacking disorder in **1-Lu**. (e) Model without stacking fault. (f) Model with stacking fault. The layer A is derived from part A, and layer B is derived from part B. In all parts: Yb1 (cyan), Yb2 (purple), Yb3a (dark blue), Lu1, Lu2 (cyan), Lu3a (light green), Lu3b (dark green), oxygen (red), and sulfur (yellow). The water molecules and the hydrogen atoms are omitted for clarity. The hydroxy groups around lutetium are omitted for clarity in e and f.

The magnetic effective moment, μ_{eff}, was derived from the following equation, $\mu_{eff} = (8C)^{0.5}$.

Heat-capacity measurements were carried out on a Quantum Design physical property measurement system (PPMS) instrument in a range of measuring magnetic fields, $0 \leq \mu_0 H \leq 14$ T. To ensure sample thermalization at low temperatures, powder measurements were made on pellets of **1-Yb** mixed with silver powder, the contribution of which was measured separately and subtracted to obtain the specific heat, C_p. The heat capacity of **1-Yb** includes three major contributions: the lattice contribution (C_l), the nuclear contribution (C_n), and the magnetic specific heat (C_m). The heat capacity of the nonmagnetic reference compound **1-Lu** was measured to subtract the specific heat from the lattice contribution (Figure S10). However, the molar heat capacity of **1-Lu** is higher than **1-Yb** above 6 K, which can be attributed to the difference between the disorder degree in these compounds. However, the values of specific heat for both compounds above 6 K are close and can be fit by the Debye law. Therefore, to exclude the lattice contribution, we assumed that $C_l = \alpha T^3$ (Debye law) when $T < 8$ K with $\alpha = 4.373$ J·K^{-4}·mol$^{-1}{}_{Yb}$ which is derived by fitting the heat capacity data of **1-Yb** from 8 to 12 K at zero field, and the lattice contribution is the same as the molar heat capacity data of **1-Yb** at zero field when $T \geq 8$ K, since the magnetic specific heat contribution should be relatively small at the higher temperature. The nuclear contribution C_n plays a dominate role when $T < 0.12$ K. However, the data points below 0.12 K are limited, which makes it hard to model the nuclear contribution accurately. The magnetic entropy is calculated by the integration of temperature dependence of C/T curve (Figure S13) from the lowest temperature.

Thermogravimetric Analysis (TGA). Thermogravimetric analysis (TGA) measurement was carried out on a Mettler Toledo instrument, TGA/DSC 3+, in the temperature range of 25−800 °C with a nitrogen flow rate of 40 mL/min.

RESULTS AND DISCUSSION

Single crystals of **1-Yb** were synthesized by the reaction of Yb_2O_3, K_2SO_4, concentrated sulfuric acid, and water in a 23 mL stainless-steel Parr vessel equipped with a Teflon liner and the subsequent heating of the Parr vessel in an oven at 210 °C for 2 days. Prismatic single crystals with dimensions of ∼0.1 mm × 0.1 mm × 0.05 mm are isolated (Figure S1) and the crystal structure of the compound was determined by single crystal X-ray diffraction (SCXRD). There are three distinct ytterbium sites in **1-Yb**, as shown in the top-left corner of Figure 1a (Yb1, Yb2, and Yb3). Site Yb3 has two possible positions (marked as Yb3a and Yb3b), and Yb3a has an occupancy of 98.58(6)% at 100 K. The Yb3b is omitted in Figure 1a−d and will be discussed later. Each ytterbium site shown in Figure 1a coordinates with seven μ_3-(OH) groups and one oxygen from SO_4^{2-}. All three sites have the same local point group symmetry (C_1) but slightly different coordination environments. These ytterbium sites assemble into two types of chains along the [100] direction. Two-thirds of the chains are straight and include Yb1 and Yb2 (designated as chain A). The other 1D chain zigzags with only Yb3a (designated as chain B). These 1D chains align in the order of "AABAABAAB..." and form Yb^{3+} layers with a triangular lattice geometry as shown in the bottom of Figure 1a and Figure 1b. There are 11 distinct distances between the nearest neighbor Yb^{3+} sites (Table S4). All the Yb_3 triangles slightly deviate from an equilateral triangle (the internal angles are shown in Table S2).

The 2D planes described by the alignment of chains A and B are not flat and have a wave-like feature (Figure 1c). The Yb−Yb−Yb angles shown in Table S3 further demonstrate this wave-like feature. The layers are connected by sulfate anions along the *b* axis, as shown in Figure 1d. Two oxygens from a sulfate anion coordinate with the adjacent Yb1 and Yb2 on one chain A and another oxygen from the same sulfate coordinates with one Yb3a in the adjacent layer. The distance between adjacent layers is 7.936 Å and is significantly larger than the average distance between the NN Yb^{3+} cations (3.661 Å), which suggests that the magnetic interactions in **1-Yb** should be mostly confined to the plane. The water molecule is located

DOI: 10.1021/acs.inorgchem.9b01674
Inorg. Chem. 2019, 58, 10417−10423

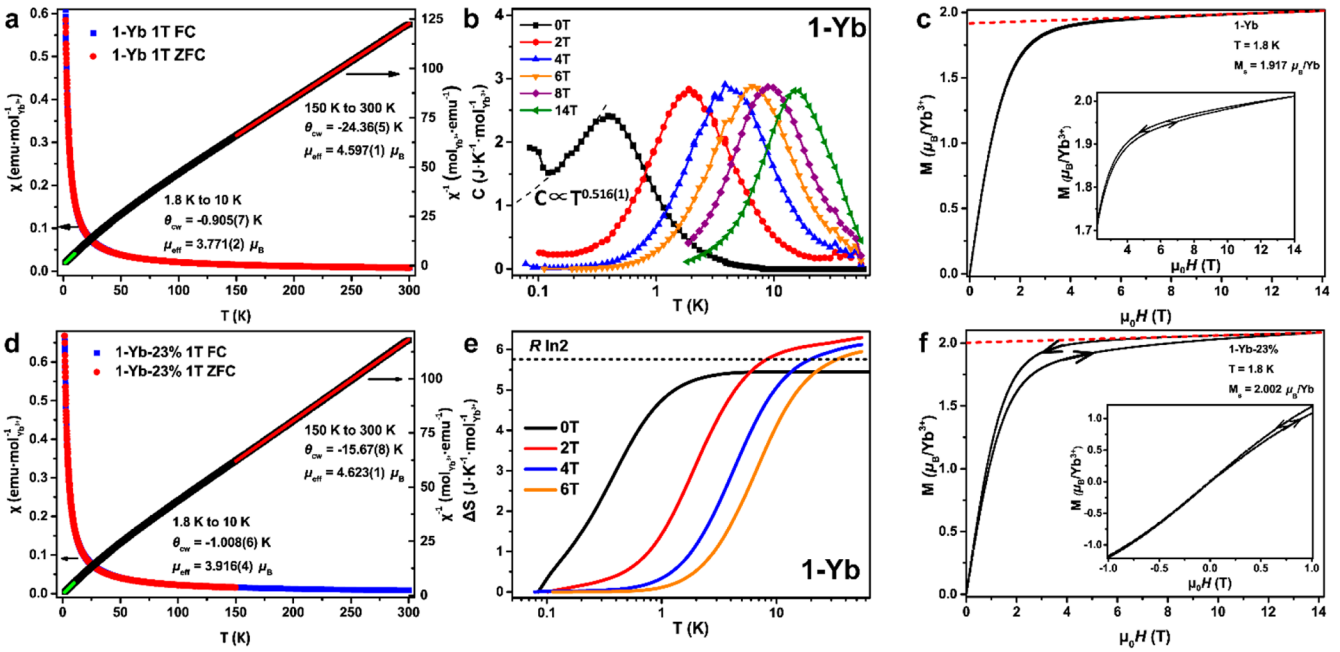

Figure 2. (a) Temperature dependence of magnetic susceptibility (left axis) and temperature dependence of inverse magnetic susceptibility (left axis) in **1-Yb** at 1 T. (b) The temperature dependence of magnetic specific heat of **1-Yb**. The dashed line represents a power law fit. (c) Magnetic field dependence of magnetization at 1.8 K in **1-Yb**. Inset: Hysteresis in the magnetic field dependence of magnetization. (d) Temperature dependence of magnetic susceptibility (left axis) and temperature dependence of inverse magnetic susceptibility (left axis) in **1-Yb-23%** at 1 T. (e) Temperature dependences of magnetic entropy in **1-Yb**. (f) Magnetic field dependence of magnetization at 1.8K in **1-Yb-23%** with hysteresis. Inset: Magnetic field dependence of magnetization from −1.0 to 1.0 T.

in three sites between layers and can be resolved in the SCXRD data.

As noted earlier, the Yb3 site in **1-Yb** has two possible positions with small atomic displacement parameters. The Yb3b site has an occupancy of 1.42(6)% at 100 K, 1.49(7)% at 252 K (Table S1), and the distance between Yb3b and Yb3a sites is 1.278(12) Å. The occupancy of the Yb3b site is too low to determine the precise chemical environment of the Yb3b site.[31] In order to understand the basis of the disorder phenomenon in **1-Yb**, the lutetium analog of this compound, **1-Lu**, was synthesized. The unit cell parameters of these two compounds are close (Table S5). The Lu3 site in **1-Lu** is similar to the Yb3 site in **1-Yb** with two split positions. However, Lu3b has an occupancy of 20.06(4)%, which enables a detailed study of the chemical environment around Lu3b. The structural model for **1-Lu** was reduced to two parts, part A with Lu3a (79.94(4)% occupancy) and part B with Lu3b (20.06(4)% occupancy), as shown in Figure S4. Part A has a similar atomic arrangement as in **1-Yb**, while part B overlaps with the part A after a translation by 3.533 Å (half of the lattice constant *a*) along the *a* axis (Table S6). Comparing the simulated PXRD patterns from part A to the experimental results, the $(10\bar{1})$, $(20\bar{2})$, and $(30\bar{3})$ reflections vanish (Figure S6), which indicates the damage of the periodicity between layers.[22,32] Therefore, the nature of the disorder in these two compounds is clearly a stacking disorder, and part A and part B can be understood as two possible positions of a single layer in the lattice as demonstrated in Figure 1e and f. The degree of disorder can be described by the occupancy of the minor part.

The degree of disorder in **1-Yb** can be adjusted by changing the ytterbium starting material. The use of $Yb_2(SO_4)_3{\cdot}8H_2O$ (instead of Yb_2O_3) and switching to an alkaline environment (addition of KOH) results in a compound with the same chemical formula as **1-Yb**, but a disorder degree of 22.83(5)% based on the SCXRD (Table S7, designated as **1-Yb-23%**). The chemical control of disorder is likely determined by the rate and temperature of formation $[Yb_x(OH)_y]^{n-}$ (Scheme S1).

The low temperature magnetic behavior of **1-Yb** is dominated by a ground-state Kramer's doublet. The magnetic susceptibility results measured under zero-field cooling (ZFC) and field cooling (FC) show no observable differences, and no long-range magnetic ordering is observed down to 1.8 K (Figure 2a). Additionally, no sharp peak or frequency dependence is found in the temperature dependence of the real part of the ac susceptibility χ' (Figure S11)—further indication that there is no spin-glass behavior above 1.8 K under zero and low fields in **1-Yb**. Fits to the high temperature portion of the inverse susceptibility data between 150 and 300 K, using the Curie−Weiss law, yield a negative Weiss temperature, θ_{cw} = −24.36(5) K and an effective moment μ_{eff} = 4.597(1) μ_B/Yb^{3+} consistent with the expected value for free Yb^{3+} ions (4.54 μ_B/Yb^{3+}). However, in this temperature regime, contributions from the crystal electric-field (CEF) excitations of Yb3+ are expected to contribute to the magnetic susceptibility.[10]

In the low temperature regime, the crystal electric-field excitations can be neglected, as indicated by the change of slope of the inverse susceptibility data around 10 K. The Curie−Weiss fit yields θ_{cw} = −0.905(7) K and μ_{eff} = 3.771(2) μ_B/Yb^{3+} for 1.8 K < *T* < 10 K, which suggests the settling of the ions into a Kramer's doublet ground state; the negative value for θ_{cw} confirms antiferromagnetic interactions between Yb^{3+} magnetic moments.[33] This assignment is further supported by the change in magnetic entropy for **1-Yb** under 2, 4, and 6 T fields, which saturates close to the *R* ln 2 value

DOI: 10.1021/acs.inorgchem.9b01674
Inorg. Chem. 2019, 58, 10417−10423

expected for a system of effective spin-1/2 moments (see Figure 2e; Materials and Methods section contains methodology). Such an effective spin-1/2 moment for Yb^{3+} is caused by the interaction between the spin−orbital coupling and CEF. We note that θ_{cw} = −0.905(7) K is about 1/4 of that in YMGO and is supported by the observed decrease in the saturation field of **1-Yb** in comparison to YMGO. While **1-Yb** is not a perfect triangular antiferromagnet, the above value of θ_{cw} yields an average antiferromagnetic $|J_1| \approx 0.60$ K for the NN exchange interaction.[34] *In toto*, these magnetic behaviors suggest that **1-Yb** displays QSL phenomenology under zero and low fields.

Heat capacity measurements were carried out to determine the collective spin ground-state of **1-Yb** samples. The magnetic contribution to C_p becomes apparent below 6 K. A plot of C with lattice contribution subtracted is shown in Figure 2b. No sharp λ-like peak can be observed under zero field, which shows no long-range ordering down to 0.08 K. The plot of C exhibits a broad peak at T = 0.45 K in zero magnetic field, and this broad peak shifts to higher temperature with increasing magnetic field. Such a shift indicates that the low temperature specific heat is predominately magnetic in origin.[4,10] Between 0.14 and 0.31 K, C (at 0 T) can be fit to a power law as $C = \alpha T^{\gamma}$ with γ = 0.516(1). Below 0.12 K, C (at 0 T) increases with decreasing temperature, which can be attributed to a nuclear contribution which has been reported in several lanthanide-based frustrated magnets.[35−37] Unfortunately, an appropriate model for the nuclear contribution cannot be applied to **1-Yb**, which affects the accuracy of the power law fit.[38] The γ = 0.516(1) is lower than the theoretical value of 0.7 reported for a triangular Heisenberg antiferromagnet with ring exchange, which might due to the existence of the nuclear contribution. However, it is still suggestive of gapless magnetic excitations for the ground state in **1-Yb**.[39]

This fractional power law parameter can also be interpreted in terms of the VBG state based on a recent theoretical study on YMGO and its analogous compound, $YbZnGaO_4$.[14,16] The existence of a VBG state under high magnetic field at low temperature can be supported by the observation of a hysteresis loop (Figure 2c) and the non-negligible divergence of FC and ZFC in the magnetic susceptibility measurement under 7 T (Figure S12). However, the hysteresis loop is not observed at low field, which indicates that the VBG state is modified by magnetic field. Such VBG states are proposed to originate from the quenched bond disorder in frustrated magnets. Since **1-Yb** presents strongly quenched disorder due to the interplay between structural distortion from an ideal triangular lattice and stacking disorder, it can serve as a unique model compound to understand the role that quenched disorder plays in ytterbium-based triangular-lattice antiferromagnets.

To understand the effect of the degree of stacking fault disorder in **1-Yb**, the magnetic properties of **1-Yb-23%** were also studied. The temperature dependence of magnetic susceptibility of **1-Yb-23%** (Figure 2d) is very similar to that of **1-Yb** with no long-range ordering occurring in the system under 1 T. An apparent change can be observed for the Curie−Weiss temperature. The θ_{cw} = −1.008(6) K value (from 1.8 to 10 K) suggests a slightly stronger antiferromagnetic interaction between NN spins in **1-Yb-23%** in comparison to **1-Yb**. A higher saturation magnetization (2.002 μ_B/Yb^{3+}) is observed in **1-Yb-23%** at 1.8 K compared to **1-Yb** (1.917 μ_B/Yb^{3+}; Figure 2f). At the same time, a more evident hysteresis loop is also observed. Additionally, a larger divergence between FC and ZFC is observed in the dc susceptibility under 7 T in **1-Yb-23%** (Figure S12). These observations all indicate that the increased stacking disorder increases the degree of quenched disorder and the magnitude of VBG state behaviors. This change may be due to the perturbation of the local coordination environment and the interlayer superexchange pathway as demonstrated by the disorder model in Figure 1e,f. It is notable that no frequency dependence of the real part of the ac susceptibility χ' under 0 T dc magnetic field are observed in **1-Yb-23%** (Figure S14), which further supports that the VBG state is modified by magnetic field.

CONCLUSIONS

In summary, a novel LRH, **1-Yb**, presenting quenched structural disorder, was synthesized. The stacking disorder in **1-Yb** is uncovered by comparing it with the lutetium analog, **1-Lu**, and the degree of disorder can be increased from 1.42(6)% to 22.83(5)% by modifying the synthetic method. The magnetic susceptibility and heat capacity results demonstrate that the as-synthesized **1-Yb** has strong frustration in the system and shows no long-range ordering down to 0.08 K. The magnetic ground state of Yb^{3+} ions is an effective spin-1/2 Kramer doublet based on the calculated effective magnetic moment, saturation magnetization, and specific heat measurements. This evidence along with the fractional power law parameter observed in specific heat suggests that the **1-Yb** displays QSL phenomenology at low field and low temperatures. Evidence for the existence of a glassy state is observed under high magnetic field and is increased in **1-Yb-23%** with a higher degree of stacking fault disorder. The chemical control of disorder in **1-Yb** provides a probe for the relationship between the quenched disorder, experimental signatures of QSL-like behavior, and the emergence of a glassy state under an applied field.

ASSOCIATED CONTENT

Supporting Information

The Supporting Information is available free of charge on the ACS Publications website at DOI: 10.1021/acs.inorgchem.9b01674.

IR spectroscopy, magnetism data, heat capacity data, TGA data and crystallographic data (PDF)

Accession Codes

CCDC 1900663−1900664, 1915839, and 1915913 contain the supplementary crystallographic data for this paper. These data can be obtained free of charge via www.ccdc.cam.ac.uk/data_request/cif, or by emailing data_request@ccdc.cam.ac.uk, or by contacting The Cambridge Crystallographic Data Centre, 12 Union Road, Cambridge CB2 1EZ, UK; fax: +44 1223 336033.

AUTHOR INFORMATION

Corresponding Author

*E-mail: la_pierre@chemistry.gatech.edu.

ORCID

Henry S. La Pierre: 0000-0002-0895-0655

Notes

The authors declare no competing financial interest.

DOI: 10.1021/acs.inorgchem.9b01674
Inorg. Chem. 2019, 58, 10417−10423

■ ACKNOWLEDGMENTS

Studies were supported by the Beckman Foundation as part of a Beckman Young Investigator Award to H.S.L. Single-crystal diffraction experiments were performed at the Georgia Institute of Technology SCXRD facility directed by Dr. John Bacsa and established with funding from the Georgia Institute of Technology. The work of M.M. and X.B. in the School of Physics (thermo-magnetic measurements) was supported by NSF-DMR-1750186. This work was performed in part at the Georgia Tech Institute for Electronics and Nanotechnology, a member of the National Nanotechnology Coordinated Infrastructure (NNCI), which is supported by the National Science Foundation (Grant ECCS-1542174). We would like to thank Marcus J. Daum for help with the magnetic property measurements.

■ REFERENCES

(1) Anderson, P. W. Resonating valence bonds: A new kind of insulator? *Mater. Res. Bull.* **1973**, *8* (2), 153−160.
(2) Anderson, P. W. The resonating valence bond state in La_2CuO_4 and superconductivity. *Science* **1987**, *235* (4793), 1196−1198.
(3) Lee, P. A. An end to the drought of quantum spin liquids. *Science* **2008**, *321* (5894), 1306−1307.
(4) Helton, J. S.; Matan, K.; Shores, M. P.; Nytko, E. A.; Bartlett, B. M.; Yoshida, Y.; Takano, Y.; Suslov, A.; Qiu, Y.; Chung, J.-H.; Nocera, D. G.; Lee, Y. S. Spin dynamics of the spin-1/2 kagome lattice antiferromagnet $ZnCu_3(OH)_6Cl_2$. *Phys. Rev. Lett.* **2007**, *98* (10), 107204.
(5) Itou, T.; Oyamada, A.; Maegawa, S.; Tamura, M.; Kato, R. Quantum spin liquid in the spin-1−2 triangular antiferromagnet $EtMe_3Sb[Pd(dmit)_2]_2$. *Phys. Rev. B: Condens. Matter Mater. Phys.* **2008**, *77* (10), 104413.
(6) Shimizu, Y.; Miyagawa, K.; Kanoda, K.; Maesato, M.; Saito, G. Spin liquid state in an organic Mott insulator with a triangular lattice. *Phys. Rev. Lett.* **2003**, *91* (10), 107001.
(7) Shores, M. P.; Nytko, E. A.; Bartlett, B. M.; Nocera, D. G. A structurally perfect S = 1/2 kagomé antiferromagnet. *J. Am. Chem. Soc.* **2005**, *127* (39), 13462−13463.
(8) Banerjee, A.; Yan, J.; Knolle, J.; Bridges, C. A.; Stone, M. B.; Lumsden, M. D.; Mandrus, D. G.; Tennant, D. A.; Moessner, R.; Nagler, S. E. Neutron scattering in the proximate quantum spin liquid α-$RuCl_3$. *Science* **2017**, *356* (6342), 1055−1059.
(9) Li, Y.; Liao, H.; Zhang, Z.; Li, S.; Jin, F.; Ling, L.; Zhang, L.; Zou, Y.; Pi, L.; Yang, Z.; Wang, J.; Wu, Z.; Zhang, Q. Gapless quantum spin liquid ground state in the two-dimensional spin-1/2 triangular antiferromagnet $YbMgGaO_4$. *Sci. Rep.* **2015**, *5*, 16419.
(10) Paddison, J. A.; Daum, M.; Dun, Z.; Ehlers, G.; Liu, Y.; Stone, M. B.; Zhou, H.; Mourigal, M. Continuous excitations of the triangular-lattice quantum spin liquid $YbMgGaO_4$. *Nat. Phys.* **2017**, *13* (2), 117−122.
(11) Shen, Y.; Li, Y.-D.; Wo, H.; Li, Y.; Shen, S.; Pan, B.; Wang, Q.; Walker, H. C.; Steffens, P.; Boehm, M.; Hao, Y.; Quintero-Castro, D. L.; Harriger, L. W.; Frontzek, M. D.; Hao, L.; Meng, S.; Zhang, Q.; Chen, G.; Zhao, J. Evidence for a spinon Fermi surface in a triangular-lattice quantum-spin-liquid candidate. *Nature* **2016**, *540* (7634), 559.
(12) Zhu, Z.; Maksimov, P.; White, S. R.; Chernyshev, A. Disorder-induced mimicry of a spin liquid in $YbMgGaO_4$. *Phys. Rev. Lett.* **2017**, *119* (15), 157201.
(13) Zhang, X.; Mahmood, F.; Daum, M.; Dun, Z.; Paddison, J. A.; Laurita, N. J.; Hong, T.; Zhou, H.; Armitage, N.; Mourigal, M. Hierarchy of Exchange Interactions in the Triangular-Lattice Spin Liquid $YbMgGaO_4$. *Phys. Rev. X* **2018**, *8* (3), 031001.
(14) Kimchi, I.; Nahum, A.; Senthil, T. Valence bonds in random quantum magnets: theory and application to $YbMgGaO_4$. *Phys. Rev. X* **2018**, *8* (3), 031028.
(15) Tarzia, M.; Biroli, G. The valence bond glass phase. *EPL (Europhysics Letters)* **2008**, *82* (6), 67008.
(16) Ma, Z.; Wang, J.; Dong, Z.-Y.; Zhang, J.; Li, S.; Zheng, S.-H.; Yu, Y.; Wang, W.; Che, L.; Ran, K.; Bao, S.; Cai, Z.; Cermak, P.; Schneidewind, A.; Yano, S.; Gardner, J. S.; Lu, X.; Yu, S.-L.; Liu, J.-M.; Li, S.; Li, J.-X.; Wen, J. Spin-glass ground state in a triangular-lattice compound $YbZnGaO_4$. *Phys. Rev. Lett.* **2018**, *120* (8), 087201.
(17) Andreanov, A.; Chalker, J. T.; Saunders, T. E.; Sherrington, D. Spin-glass transition in geometrically frustrated antiferromagnets with weak disorder. *Phys. Rev. B: Condens. Matter Mater. Phys.* **2010**, *81* (1), 014406.
(18) Balents, L. Spin liquids in frustrated magnets. *Nature* **2010**, *464* (7286), 199.
(19) Shores, M. P.; Nytko, E. A.; Bartlett, B. M.; Nocera, D. G. A structurally perfect S = 1/2 kagome antiferromagnet. *J. Am. Chem. Soc.* **2005**, *127* (39), 13462−13463.
(20) Savary, L.; Balents, L. Quantum spin liquids: a review. *Rep. Prog. Phys.* **2017**, *80* (1), 016502.
(21) Rozenberg, M. J.; Chitra, R. Disorder effects in the quantum kagome antiferromagnet $ZnCu_3(OH)_6Cl_2$. *Phys. Rev. B: Condens. Matter Mater. Phys.* **2008**, *78* (13), 132406.
(22) Bette, S.; Takayama, T.; Kitagawa, K.; Takano, R.; Takagi, H.; Dinnebier, R. E. Solution of the heavily stacking faulted crystal structure of the honeycomb iridate $H_3LiIr_2O_6$. *Dalton Trans.* **2017**, *46* (44), 15216−15227.
(23) Kitagawa, K.; Takayama, T.; Matsumoto, Y.; Kato, A.; Takano, R.; Kishimoto, Y.; Bette, S.; Dinnebier, R.; Jackeli, G.; Takagi, H. A spin-orbital-entangled quantum liquid on a honeycomb lattice. *Nature* **2018**, *554* (7692), 341.
(24) Slagle, K.; Choi, W.; Chern, L. E.; Kim, Y. B. Theory of a quantum spin liquid in the hydrogen-intercalated honeycomb iridate $H_3LiIr_2O_6$. *Phys. Rev. B: Condens. Matter Mater. Phys.* **2018**, *97* (11), 115159.
(25) Geng, F.; Ma, R.; Sasaki, T. Anion-exchangeable layered materials based on rare-earth phosphors: unique combination of rare-earth host and exchangeable anions. *Acc. Chem. Res.* **2010**, *43* (9), 1177−1185.
(26) Zhu, Q.; Wang, X.; Li, J.-G. Recent progress in layered rare-earth hydroxide (LRH) and its application in luminescence. *J. Adv. Ceram.* **2017**, *6* (3), 177−186.
(27) Li, H.; Sheng, T.; Xue, Z.; Zhu, X.; Hu, S.; Wen, Y.; Fu, R.; Zhuo, C.; Wu, X. Synthesis, structure, characterization, and multifunctional properties of a family of rare earth organic frameworks. *CrystEngComm* **2017**, *19* (15), 2106−2112.
(28) Sheldrick, G. M. *SADABS*; Bruker AXS Inc.: Madison, WI, 1996.
(29) Sheldrick, G. M. A short history of SHELX. *Acta Crystallogr., Sect. A: Found. Crystallogr.* **2008**, *64* (1), 112−122.
(30) Sheldrick, G. M. Crystal structure refinement with SHELXL. *Acta Crystallogr., Sect. C: Struct. Chem.* **2015**, *71* (1), 3−8.
(31) But it should be noted that the occupancy of disorder is independent of temperature, which is proven by the crystal structure of **1-Yb** measured under 252 K, **1-Yb-252K**, with an occupancy of 1.49(7)% for the Yb3b site.
(32) Cadars, S.; Allix, M.; Brouwer, D. H.; Shayib, R.; Suchomel, M.; Garaga, M. N.; Rakhmatullin, A.; Burton, A. W.; Zones, S. I.; Massiot, D.; Chmelka, B. F. Long-and short-range constraints for the structure determination of layered silicates with stacking disorder. *Chem. Mater.* **2014**, *26* (24), 6994−7008.
(33) Bramwell, S.; Field, M.; Harris, M.; Parkin, I. Bulk magnetization of the heavy rare earth titanate pyrochlores-a series of model frustrated magnets. *J. Phys.: Condens. Matter* **2000**, *12* (4), 483.
(34) Ding, L.; Manuel, P.; Bachus, S.; Grußler, F.; Gegenwart, P.; Singleton, J.; Johnson, R. D.; Walker, H. C.; Adroja, D. T.; Hillier, A. D. Gapless spin-liquid state in the structurally disorder-free triangular antiferromagnet $NaYbO_2$. *arXiv preprint*, arXiv:1901.07810, **2019**.
(35) Paddison, J. A.; Ong, H. S.; Hamp, J. O.; Mukherjee, P.; Bai, X.; Tucker, M. G.; Butch, N. P.; Castelnovo, C.; Mourigal, M.; Dutton, S. E. Emergent order in the kagome Ising magnet $Dy_3Mg_2Sb_3O_{14}$. *Nat. Commun.* **2016**, *7*, 13842.

DOI: 10.1021/acs.inorgchem.9b01674
Inorg. Chem. 2019, 58, 10417−10423

(36) Dun, Z. L.; Li, X.; Freitas, R. S.; Arrighi, E.; Dela Cruz, C. R.; Lee, M.; Choi, E. S.; Cao, H. B.; Silverstein, H. J.; Wiebe, C. R.; Cheng, J. G.; Zhou, H. D. Antiferromagnetic order in the pyrochlores $R_2Ge_2O_7$ (R= Er, Yb). *Phys. Rev. B: Condens. Matter Mater. Phys.* **2015**, *92* (14), 140407.
(37) Matsumoto, Y.; Nakatsuji, S.; Kuga, K.; Karaki, Y.; Horie, N.; Shimura, Y.; Sakakibara, T.; Nevidomskyy, A. H.; Coleman, P. Quantum criticality without tuning in the mixed valence compound β-$YbAlB_4$. *Science* **2011**, *331* (6015), 316−319.
(38) The lack of lower temperature data for specific heat under zero field hinders the determination of the nuclear contribution in this system.
(39) Motrunich, O. I. Variational study of triangular lattice spin-1−2 model with ring exchanges and spin liquid state in $\kappa(ET)_2Cu_2(CN)_3$. *Phys. Rev. B: Condens. Matter Mater. Phys.* **2005**, *72* (4), 045105.

DOI: 10.1021/acs.inorgchem.9b01674
Inorg. Chem. 2019, 58, 10417−10423